Acta Materialia 122 (2017) 11–18

Contents lists available at ScienceDirect

Acta Materialia

journal homepage: www.elsevier.com/locate/actamat

Full length article

An assessment of the lattice strain in the CrMnFeCoNi high-entropy alloy

L.R. Owen [a, b], E.J. Pickering [c], H.Y. Playford [b], H.J. Stone [a], M.G. Tucker [d], N.G. Jones [a, *]

[a] Department of Materials Science and Metallurgy, University of Cambridge, 27 Charles Babbage Road, Cambridge, CB3 0FS, UK
[b] STFC ISIS Facility, Rutherford Appleton Laboratory, Didcot, OX11 0QX, UK
[c] School of Materials, University of Manchester, Oxford Road, Manchester, M13 9PL, UK
[d] Spallation Neutron Source, Oak Ridge National Laboratory, Oak Ridge, TN, USA

ARTICLE INFO

Article history:
Received 10 May 2016
Received in revised form
29 July 2016
Accepted 19 September 2016

Keywords:
High-entropy alloys
Neutron diffraction
Lattice strains
Pair correlation function

ABSTRACT

The formation of single phase solid solutions from combinations of multiple principal elements, with differing atomic radii, has led to the suggestion that the lattices of high-entropy alloys (HEAs) must be severely distorted. To assess this hypothesis, total scattering measurements using neutron radiation have been performed on the CrMnFeCoNi alloy and compared with similar data from five compositionally simpler materials within the same system. The Bragg diffraction patterns from all of the studied materials were similar, consistent with a face-centered cubic structure, and none showed the pronounced dampening that would be expected from a highly distorted lattice. A more detailed evaluation of the local lattice strain was made by considering the first six coordination shells in the pair distribution functions (PDF), obtained from the total scattering data. Across this range, the HEA exhibited the broadest PDF peaks but these widths were not disproportionately larger than those of the simpler alloys. In addition, of all the materials considered, the HEA was at the highest homologous temperature, and hence the thermal vibrations of the atoms would be greatest. Consequently, the level of local lattice strain required to rationalise a given PDF peak width would be reduced. As a result, the data presented in this study do not indicate that the local lattice strain in the equiatomic CrMnFeCoNi HEA is anomalously large.

1. Introduction

High-Entropy Alloys (HEAs) differ from conventional metallic materials in that they are based upon multiple atomic species in near equiatomic ratios, rather than a single principal element. It might be expected that the microstructures of these alloys would contain several intermetallic phases, but much of the literature associated with these materials has reported only solid solutions with simple crystal structures, such as face- or body-centered cubic (fcc and bcc respectively) and their related superlattice structures [1,2]. These observations have given rise to the concept of entropic stabilisation, which suggests that the configurational entropy of these multi-component solid solutions can overcome the enthalpy of formation of competing intermetallic phases [1]. However, whilst initially appealing, caution should be exercised as several datasets have been obtained from as-fabricated material, which is likely to have been in a metastable state, as opposed to the thermodynamic equilibrium achieved by homogenisation and long duration thermal exposures [1–7]. In addition, studies using higher-resolution techniques have also revealed the presence of nano-scale precipitates in some alloys [8,9].

Nevertheless, the formation of statistically disordered single phase multi-component solid solutions is interesting, as the arrangement of the different atomic species will be far more complex than in a conventional dilute alloy. For example, in a relatively simple austenitic stainless steel, such as Fe–18Cr–8Ni wt.%, almost 75% of the atoms surrounding any given lattice site would be Fe. Conversely, in a five-component equiatomic HEA that also adopts an fcc structure, only 20% of the nearest neighbours would be atoms of the same species. This complicated arrangement of multiple atom types, each with a different size and electronic structure, is directly related to two of the four proposed HEA core effects; sluggish diffusion and severely distorted lattices [2,10,11]. Limited evidence exists for either of these effects, but data relating

* Corresponding author.
E-mail address: ngj22@cam.ac.uk (N.G. Jones).

http://dx.doi.org/10.1016/j.actamat.2016.09.032

to the lattice distortion in the literature is particularly sparse and hence forms the basis of the current work [12].

It is well established that the addition of alloying elements into a pure metal causes local distortions in the regular atomic array, moving neighbouring host atoms away from their ideal positions. The strain fields associated with these distortions impede gliding dislocations, giving rise to strengthening. These concepts have been extended to the multi-component HEAs, where it has been suggested that the cumulative effect of a significant number of different atom types within the first coordination shell would generate a highly strained structure [2]. Such severely distorted arrays could give rise to a significant level of solid solution strengthening, as has been reported in a number of HEA systems [3,13–15]. However, strength could also have been influenced by the presence of nano-scale precipitates within the material and significant levels of strain would be expected to destabilise the lattice, resulting in precipitation or amorphisation [16–18]. Thus, there is an obvious need to obtain new data that can clarify this matter.

One reason for the lack of clear experimental data that elucidates the extent of the lattice distortions in HEAs is the difficulty in making suitable measurements. High-resolution transmission electron microscopy imaging of the atomic columns can show local distortions [19]. However, images of this type display an average of the signal along each atom column and are susceptible to distortions caused by other effects, such as damage caused during ion beam thinning. In diffraction experiments, the displacement of atoms away from their ideal positions would affect the observed peak intensities, in a similar manner to thermal vibrations [20,21]. Larger distortions would reduce the intensity of each diffraction peak, with that signal becoming redistributed into diffuse scattering. Several publications have presented data showing this effect [2,3,11,13,15,22,23], but the most comprehensive example is Fig. 11 in Ref. [11], which presents a series of single phase, fcc alloys with systematically increasing chemical complexity. However, lattice distortions are not the only factor that can cause a reduction in the observed peak intensity, particularly when comparing different samples measured on a laboratory diffractometer. Factors such as crystallographic texture (or lack of powder average statistics), the fluorescence of certain atomic species when irradiated by particular incident photons, and other instrumental effects would all influence the intensity of a diffraction peak. Thus, without accounting for these effects, it cannot be conclusively determined whether the atomic arrays in single phase multi-component solid solutions are severely distorted.

Recently, it has been suggested that the use of total scattering data can provide more information on the nature of the local arrangements and positions of the atoms in HEAs [24–26]. Total scattering is an extension of traditional powder diffraction measurements, wherein both Bragg and diffuse scattering are measured and analysed simultaneously. The Fourier transform of total scattering data produces a pair distribution function (PDF), which is a weighted histogram of the interatomic distances within the irradiated volume. The position and shape of the peaks in a PDF provide information on the local environment surrounding each atom, as opposed to the average structural information contained within the Bragg data. Total scattering measurements have been made on a ZrNbHf ternary alloy and an $Al_{1.3}$CoCrCuFeNi HEA using both X-ray and neutron radiation [24–26]. These studies have identified that the shape of the PDF peaks at short interatomic distance varied from those expected from an ideal structure and these differences were attributed to the presence of local distortions in the lattice. However, in both cases, the samples were measured in the as-cast condition, which is likely to contain solidification induced microsegregation that could affect the PDF peak shape. Similarly, the pronounced crystallographic texture displayed in the ZrNbHf sample and the complex three-phase microstructure of the $Al_{1.3}$CoCrCuFeNi HEA, would need to be accounted for, to provide an in depth understanding of the strain in these alloys [27]. Therefore, whilst these studies clearly illustrate the capability of the technique, further measurements, with careful consideration of sample complexity and condition, are required to provide a clear picture of the local environment in HEAs.

To address this issue, here we present total scattering measurements made with neutron radiation on a five-component equiatomic powder HEA sample in a single-phase condition. The sample was gas atomised to ensure that good powder diffraction data could be obtained and textural effects avoided [27]. The results are compared to data for a Ni powder, three Ni-Cr binary alloys and a Ni-Co-Cr ternary alloy. Whilst the results indicate that the strain in the HEA lattice is greater than that of pure Ni, the magnitude of this strain was similar to that observed in some of the binary and ternary alloys and cannot be considered anomalously large. As such, the data reported here do not support the overarching concept that all multi-component solid solutions must have severely distorted lattices.

2. Experimental methods

Gas atomised powders of Ni-33Cr (at.%) and an equiatomic CrMnFeCoNi HEA were produced by Hauner Metallische Werkstoffe. A small quantity of each powder was encapsulated within an evacuated and Ar backfilled quartz tube prior to heat treatment at 1200 °C for 2 h followed by water quenching. The heat treatment served to both chemically homogenise the material and sinter the powders into a bar. The surfaces of the sintered bars were lightly ground to remove any potential contamination from the heat treatment process.

Total scattering measurements were performed on the Polaris instrument at the ISIS Neutron and Muon Source (RB1520332 (December 2015)). To ensure that data of sufficient quality were acquired, these measurements were made for a total of 4 h under ambient conditions. The scattering data were focussed using the Mantid software [28], which corrected, normalised and collated the information from the 3008 detectors. Rietveld refinement of the Bragg data was performed using the GSAS program [29]. The total scattering data were processed using the GudrunN software [30] and Fourier transformed to obtain pair distribution functions using the SToG program, distributed as part of the RMCProfile package [31], with a $Q_{max} = 31$ Å^{-1}. Modelling of the total scattering data was also performed using the RMCProfile program.

The data collected were compared to data gathered previously under the same conditions on the Polaris instrument for Ni, Ni-20Cr, Ni-25Cr (RB1510579 (May 2015)) and Ni-37.5Co-25Cr (RB1310308 (May 2014)). The Ni was investigated in the as-received powder form, whilst the alloy specimens were all fabricated using the same method as described above but with different heat treatment parameters. The Ni-Cr binaries were heat treated for 100 h at 1000 °C, whilst the Ni-37.5Co-25Cr alloy was exposed for 100 h at 900 °C. In addition, the sintered Ni-37.5Co-25Cr alloy bar was crushed using a hand percussion mill prior to the scattering measurement. All of the data from previous experiments were reanalysed together with that from the current experiment to ensure consistency of data handling.

3. Results

The neutron diffraction patterns from the different alloys are shown in Fig. 1. The raw data underwent standard normalisation against pure vanadium to account for the incident neutron flux on

the sample. In Fig. 1, the data have also been scaled by the intensity of the $\{111\}_{Ni}$ peak to facilitate comparison of the different datasets. The data indicated that in the studied condition all of the samples were single phase materials with an fcc structure. The one exception to this was the Ni sample, which contained a small volume fraction (~2.5%) of nickel oxide, evidence of which can be seen by the small reflection at a *d*-spacing just below 1.5 Å (indicated by an arrow in the figure).

Rietveld refinements of the powder diffraction patterns were performed using the GSAS software [29], and an example of a fitted dataset is given in Fig. 2. This dataset corresponds to the HEA sample and the quality of the fit is indicative of all of the other refinements. As can be seen from Fig. 2, the entire pattern was well described by the model, which indicated that the crystallites in the sintered bars represented an adequate powder average. As a result, the intensities of the diffraction peaks are directly related to the

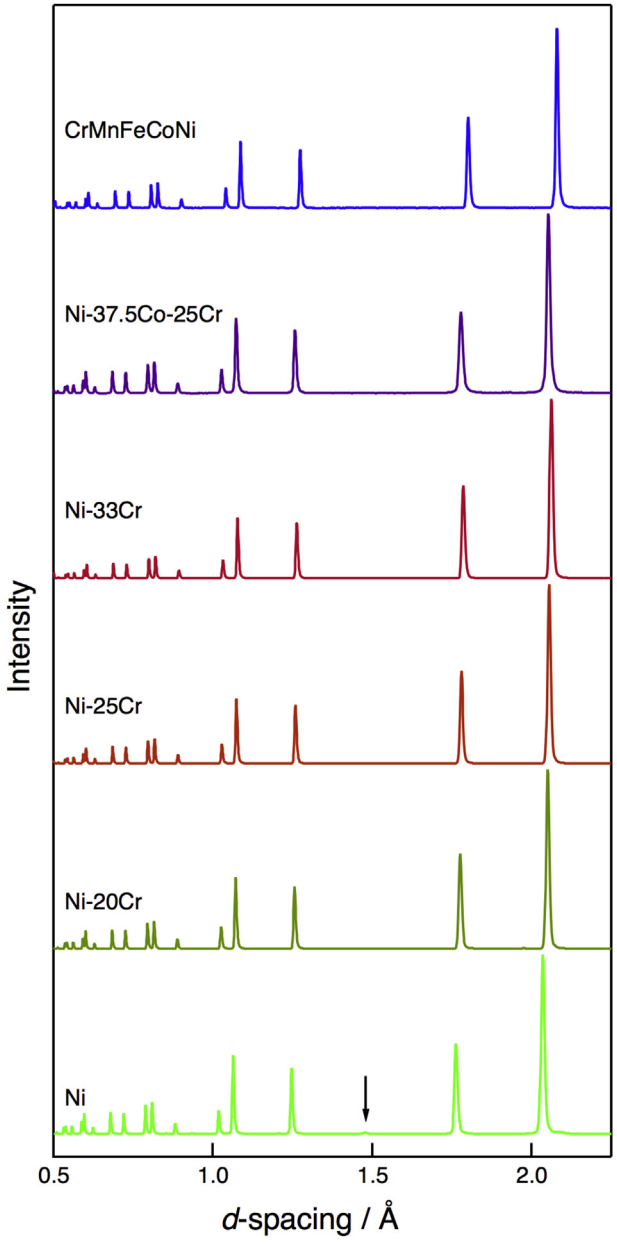

Fig. 1. Normalised and scaled neutron diffraction patterns of the studied alloys. The arrow indicates the presence of a NiO impurity in the Ni sample.

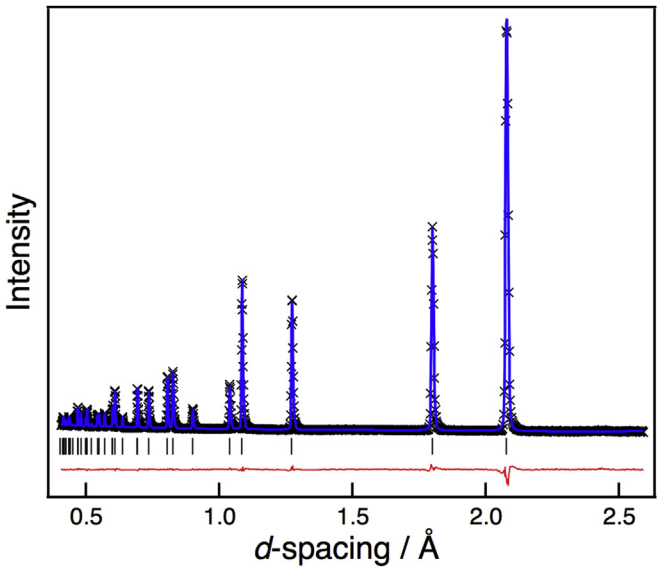

Fig. 2. Rietveld refined neutron powder diffraction pattern from the CrMnFeCoNi HEA, with markers for the experimental data, the overall fit shown in blue and the residuals shown by the red line. (For interpretation of the references to colour in this figure legend, the reader is referred to the web version of this article.)

atom types and their locations within the unit cell. Rietveld refinement of the solid solution phases assumes that the constituent elements are randomly distributed across the lattice sites. Therefore, the excellent fits obtained for each material indicated that the diffraction data were entirely consistent with this model. However, evaluation of the Bragg data, for any system, assesses the average structure of the material and does not provide any information about local effects around each atom.

The refined lattice parameter (a) and the isotropic thermal motion factor (U_{iso}) for each alloy, along with the melting temperatures, are given in Table 1. When the data corresponding to the Ni and Ni-Cr binary alloys were considered, then the expected linear expansion of the lattice parameter with increasing Cr content was observed, in line with a hard sphere model. However, neither the refined lattice parameters of the ternary alloy nor the HEA were well described by extending this simple model. The U_{iso} values, provided in Table 1, describe a *d*-spacing dependent modification to intensity that accounts for thermal motion of the atoms about their ideal position, i.e. dynamic displacements. Local lattice strain, which is the static displacement of an atom away from its ideal position, is known to produce diffuse scattering similar to that of thermal motion, with a corresponding reduction in the intensity of the Bragg peaks [32]. Therefore, within a Rietveld refinement both static and dynamic displacements are subsumed within the U_{iso}

Table 1
Rietveld refined lattice parameters (a) and isotropic thermal motion factors (U_{iso}) for all of the studied materials along with their melting temperatures (T_m). The errors in the lattice parameter values were less than 0.0001 Å and less then 0.06×10^{-3} for the U_{iso} terms. Values for T_m were obtained from ThermoCalc using the TTNi5 Database, with the exception of CrMnFeCoNi, which was taken from Ref. [35].

Alloy (at.%)	a (Å)	U_{iso} (Å^2)	T_m (K)
Ni	3.520	4.59×10^{-3}	1728
Ni-20Cr	3.547	4.92×10^{-3}	1695
Ni-25Cr	3.555	4.83×10^{-3}	1686
Ni-33Cr	3.567	5.02×10^{-3}	1667
Ni-37.5Co-25Cr	3.551	4.49×10^{-3}	1725
CrMnFeCoNi	3.597	5.46×10^{-3}	1543

term. Whilst the refined HEA dataset did produce the largest U_{iso} value, no obvious correlation could be seen between compositional complexity and the refined U_{iso} values when considering all of the different datasets.

Total scattering measurements allow the assessment of a material at a local atomic level, as opposed to the average description of the structure achieved through Bragg data. The pair distribution function (PDF), which can be obtained from total scattering data, is a weighted average of the distances between atoms within a given structure and, therefore, can provide insight into the distribution of interatomic distances. The PDFs for each of the alloys studied are shown in Fig. 3. In all cases, the form of the PDF was typical of an fcc lattice, in good agreement with the Bragg data. On initial inspection, no difference could be determined between the datasets, save the systematic shift of the peak position in r consistent with the variation of the lattice parameters. In addition, all of the PDFs exhibited a similar dampening of the peak amplitudes as a function of r.

To obtain quantitative information from a PDF, a model of the structure must be created that is capable of accurately describing the experimental data. In the present work, this was achieved using a large box model and the reverse Monte-Carlo algorithm. Critically, all of the datasets were modelled using boxes containing only a single atom type, termed a grey atom, which had a compositionally weighted average scattering length of all the constituent elements. Fig. 4 shows the PDF of the HEA sample fitted in this way. As can be seen, the quality of the fit is extremely good, demonstrating that the system was well described by a grey atom model. As a consequence, the distribution of atoms on a local scale was also likely to be random, in agreement with the average structure determined from the Bragg data. The fits to all the other datasets were of at least comparable, if not higher, quality than that shown in Fig. 4, leading to the conclusion that all of the studied materials were statistically random solid solutions with an fcc structure.

4. Discussion

To understand the implications of a severely strained multi-component lattice and how it might manifest itself in experimental measurements, it is necessary to first consider a pure element and simpler solid solution systems. For a pure element, such as Ni, in an idealised dislocation free condition, it is envisaged that all atoms undergo thermal oscillations about the lattice points. This would lead to a normal distribution of the observed bond lengths and hence a Gaussian form to the PDF peaks. The incorporation of an alloying addition into the lattice, such as a larger Cr atom, would produce a local strain field as a result of the size mismatch between the two species, displacing the surrounding host atoms from their ideal positions. It would be anticipated that in a statistically random solid solution these static displacements would result in a broadening of the peaks in the corresponding PDF and a reduction in the intensity of the Bragg peaks.

Both the Rietveld refinement of the Bragg data and the reverse Monte-Carlo simulations of the PDFs suggested that all of the studied samples were in a single phase condition and were statistically disordered. As a consequence, the potential influence of chemical inhomogeneity and crystallographic orientation on the data need not be considered. Therefore, following the logic above, alloys with greater lattice strain would be expected to exhibit more pronounced dampening of their diffraction peaks. Simple inspection of the Bragg diffraction patterns in Fig. 1 showed no obvious change in the peak dampening between any of the alloys. Mathematically, a dampening of this type would be captured within the U_{iso} term of a Rietveld refinement. However, whilst there was variation between the refined U_{iso} values for the different alloys, there was no clear trend in relation to their compositional complexity. In particular, the refined U_{iso} value for the Ni-37.5Co-25Cr alloy was lower than any of the binary Ni-Cr alloys or pure Ni. Whilst the relationship between local lattice strain and Bragg

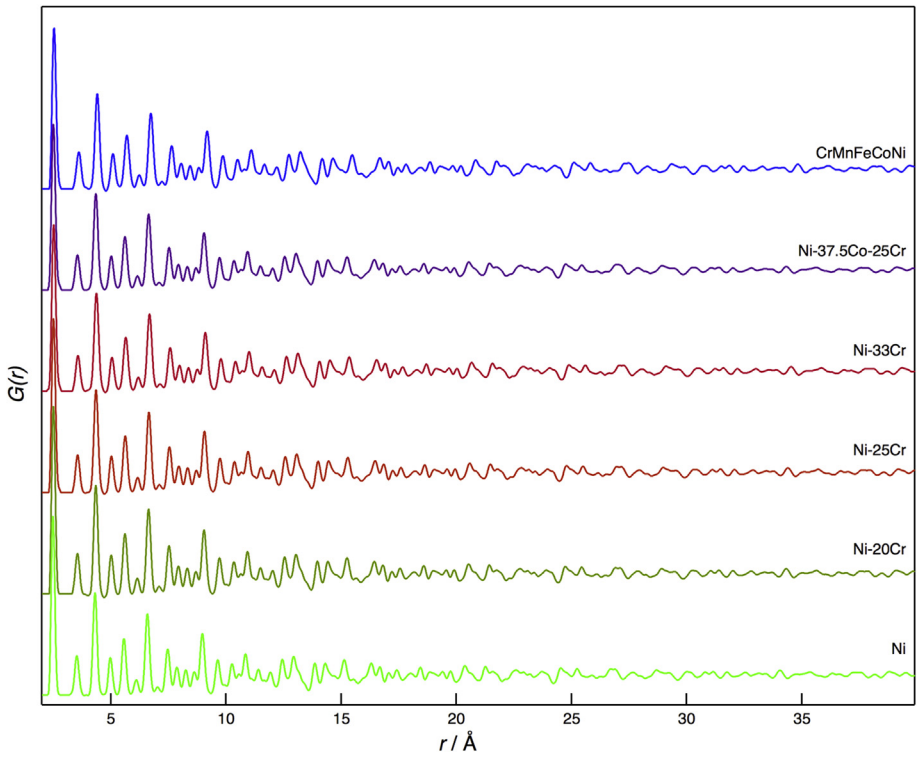

Fig. 3. Normalised pair distributions functions (G(r)) for all of the studied alloys.

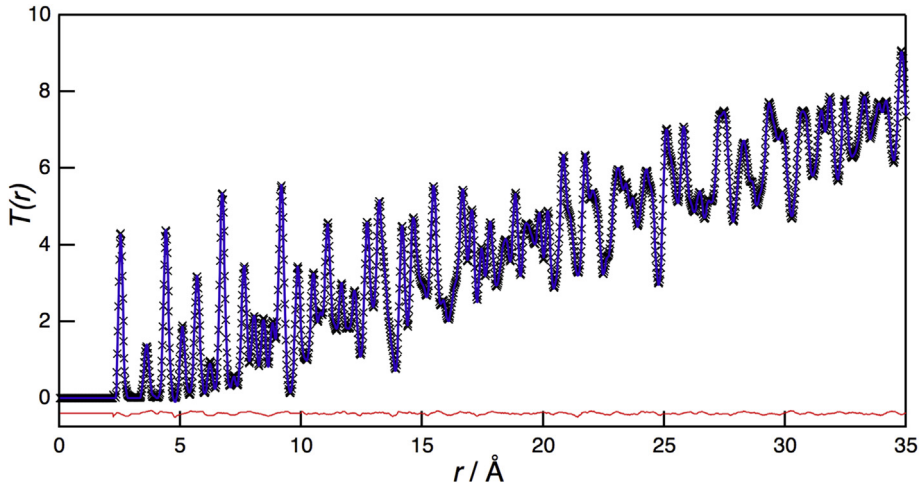

Fig. 4. A fitted pair distribution function (T(*r*)) for CrMnFeCoNi. Experimental data shown by markers, fitted data from a reverse Monte-Carlo refinement using a grey atom model shown in blue and the difference curve shown in red. (For interpretation of the references to colour in this figure legend, the reader is referred to the web version of this article.)

dampening is theoretically sound, to make any meaningful comment about the magnitude of this strain would require the deconvolution of the U_{iso} term into both static and dynamic components.

All samples were measured at room temperature and were therefore subjected to the same thermal energy. However, the magnitude of the thermal vibrations are a function of this energy and the elastic constants of the material, which themselves are related to the melting temperature [33]. Thus, the amplitude of thermal vibrations around a lattice site will be smaller in a material at a lower homologous temperature. This effect appears to show a better correlation to the refined U_{iso} values than compositional complexity, especially when considering the low U_{iso} value of the Ni-37.5Co-25Cr sample. This suggests that dynamic displacements may be dominating the refined U_{iso} values of all the materials, meaning the local static displacements in the HEA may not be as large as hypothesised. However, given the difficulty in separating these two effects, it is suggested that the assessment of Bragg dampening alone is not sufficient to provide conclusive evidence with regard to the level of local lattice strain.

The analysis of a PDF, constructed from total scattering data, provides information at the local level and, therefore, should be more suitable for assessing the lattice strains. Each peak in a PDF corresponds to a coordination shell around an atom, at a radius of *r*, and the area is dependent on the coordination number and interacting atomic species. A distorted lattice would be expected to increase the width of every peak in the PDF as the atoms are displaced from their ideal positions. If these displacements are significant in the low *r* coordination shells, then the cumulative effect at larger values of *r* would cause the peaks to become so broad that they lose their form, potentially leading to a featureless PDF at high *r*. Considering the data presented in Fig. 3, no obvious difference can be seen between the different materials studied and good peak definition can be observed over the complete *r* range. This suggests that all of the materials have well defined lattices, with no significant distortion. However, to study the effect of local lattice strains in more detail, analysis of the first six coordination shells was performed. The corresponding region of the G(*r*) PDF, Fig. 3, has been expanded for clarity in Fig. 5. Again, with the exception of the positional shift in *r*, associated with the different lattice parameters, the form of these functions appears identical.

The width of a PDF peak is a function of the static and dynamic displacements of the atoms within the crystal, the Q_{max} of the Fourier transform and the inherent instrumental effects. All of the data reported in this study were acquired using the same instrument and, therefore, with only small differences in the lattice parameters of each material, the inherent broadening should be essentially identical and can effectively be ignored. The static component of sample broadening will depend on the dislocation density of the material, surface effects and any local lattice strains corresponding to the displacements of atoms away from their ideal locations. The dynamic component of sample broadening, as with Bragg data, is solely related to the thermal vibrations of the atoms about their positions. All of the alloys considered in this study were subjected to elevated temperature heat treatments prior to investigation, which should have minimised the dislocation densities and relieved any local strains caused by the atomisation process. The Ni-37.5Co-25Cr alloy was crushed following heat treatment, which could have introduced dislocations and may need to be accounted for in subsequent analysis. Surface effects would only be expected to be significant if the crystals were extremely small, such that their surface to volume ratio was high. Given that all of the alloys were exposed to temperatures in excess of 900 °C for reasonable lengths of time, nanometer sized crystals seem unlikely. Thus, in the present work, it is believed that the thermal vibrations and local lattice strains dominate the observed PDF peak widths.

Visual inspection of Fig. 5 reveals no obvious variation in the breadth of the PDF peaks between the different alloys, but to assess this more accurately each peak was fitted with a Gaussian function. The fitted values of full width at half maximum (FWHM) for all six peaks from each alloy are shown in Fig. 6. No clear trend with respect to the relationship between PDF peak width and composition can be seen across all coordination shells. The FWHM values from the first coordination shell are always the lowest, whilst those corresponding to the other coordination shells are, broadly speaking, of similar magnitudes. This effect on the first coordination shell is believed to be a result of correlated motion between different pairs of nearest neighbouring interacting atoms [34].

It would be expected that a monatomic sample would exhibit the narrowest PDF peaks, as there are no compositionally associated lattice strains. As such, the thermal motion of the atoms should dominate the widths of the PDF peaks. Surprisingly, this was not the case in the experimental data, where Ni-20Cr was observed to have the narrowest PDF peaks in all but the fifth coordination shell. This observation could either suggest that some form of ordering was present within the Ni-20Cr sample, or that the Ni

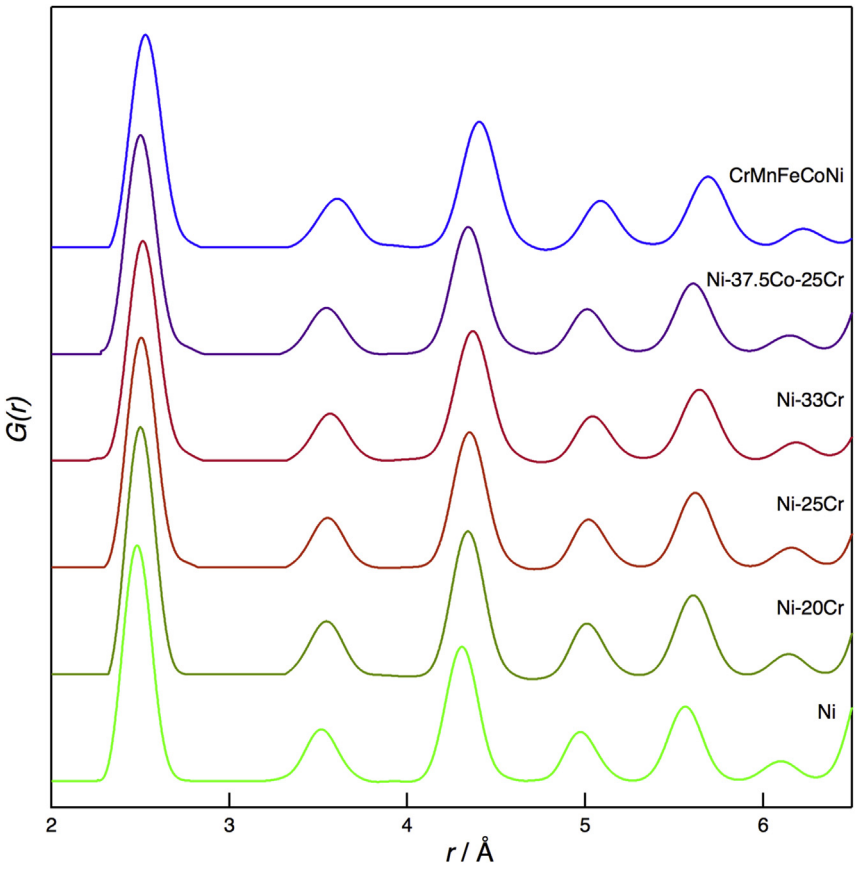

Fig. 5. Normalised pair distribution functions (G(r)) for all of the studied alloys limited to the first six coordination shells.

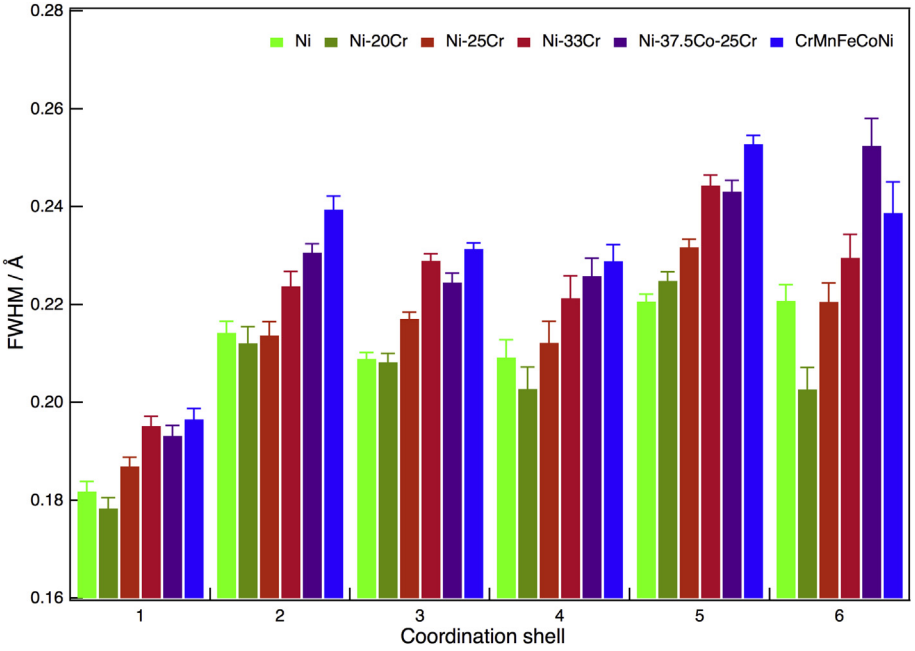

Fig. 6. Full width at half maximum (FWHM) values from Gaussian fits to the first six peaks of the pair distribution (G(r)) function of each alloy.

sample contained some static displacements. Since the Ni powder was studied in the as-received condition, with no knowledge of the prior processing history, and was found to contain a small fraction of NiO, the latter seems more likely.

The three Ni-Cr alloys showed a systematic increase in PDF peak width with greater Cr concentration. In terms of static displacements this trend is expected as, in addition to the expansion of the lattice, the local positions of the solvent atoms alter to

accommodate a greater concentration of the larger solute atoms. A similar effect was also observed for the Ni-37.5Co-25Cr ternary alloy, where the substitution of Co for Ni resulted in broader PDF peaks than the Ni-25Cr binary alloy. This observation suggested that there was a greater level of strain in the lattice of ternary alloy than in the binary alloy with the same Cr concentration. In all but the sixth coordination shell, the HEA exhibited the greatest PDF peak widths, suggesting that this lattice contained the greatest level of local strain of all the alloys considered. However, in several of the coordination shells, the magnitudes of HEA PDF peak widths were comparable to those of either Ni-33Cr or Ni-37.5Co-25Cr. Thus, whilst it is clear that the HEA lattice contained some level of local strain, it did not appear to be disproportionately larger than those found in the lattices of other, compositionally simpler alloys.

Whilst the discussion above seems to provide a logical explanation for the observed PDF peak widths, it implicitly assumed that the magnitude of the dynamic displacements were constant for all alloys. As previously discussed, the variation in U_{iso} terms obtained from the Bragg data showed a correlation between the magnitude of the thermal motion and the melting temperatures, meaning that the dynamic displacements cannot be considered constant at any given temperature.

From the melting temperatures provide in Table 1, the broadening of the PDF peaks due to thermal motion would be expected to increase in the following order: Ni, Ni-37.5Co-25Cr, Ni-20Cr, Ni-25Cr, Ni-33Cr and CrMnFeCoNi. Considering thermally driven dynamic displacements only, the trend in the breadth of the PDF peaks is well described with the exception of the Ni and the Ni-37.5Co-25Cr samples, both of which exhibited broader peaks than would be expected. Therefore, these samples must contain a significant static displacement in order to produce such broad PDF peaks. As stated above, the processing history of the Ni sample was unknown and the Ni-37.5Co-25Cr was crushed following heat treatment, both of which could lead to increased static displacements, thereby rationalising the observed PDF peak breadth. Consequently, these observations indicate that the breadth of the PDF peak observed for the HEA sample is not necessarily dominated by static displacements.

As quantification of the static displacements present within a lattice is extremely challenging, the expected level of strain is often related to the magnitude of the variation in atomic radii. A common method by which this has been assessed is through the evaluation of δr using the following expression, where r_i is the radius of an individual atomic species and c_i is its concentration.

$$\delta r = \sqrt{\sum c_i \left(1 - \frac{r_i}{r_{av}}\right)^2}$$

$$r_{av} = \sum c_i r_i$$

Using this expression to assess the difference in atomic radii of the alloys studied in this work yields the following results: $\delta r = 0.0115$ for Ni-20Cr; $\delta r = 0.0124$ for Ni-25Cr; $\delta r = 0.0134$ for Ni-33Cr; $\delta r = 0.0122$ for Ni-37.5Co-25Cr and $\delta r = 0.0106$ for CrMnFeCoNi. There are two key points that should be noted from these values. First, none of these alloys have particularly large differences in atomic radius, all having a $\delta r < 0.015$ (1.5%). Second, the δr value of CrMnFeCoNi is the lowest. Consequently, the lattice of CrMnFeCoNi would not be expected to contain large static displacements.

The PDF peak width appears to vary approximately linearly with δr, as the Cr concentration of the Ni-Cr binary alloys increases but, as with similar calculations of lattice parameter (*i.e.* Vegard's Law), the addition of ternary or higher order additions breaks this simple trend. It is likely that this limitation is due to the simplicity of a hard sphere type approach, in particular the fact that it does not consider how the bond energies may change with different atomic species or the effect of temperature.

If the magnitudes of the thermal vibrations are assumed to be constant, then the change of the PDF peak width between the different samples can be attributed to variations in static displacements. In the first coordination shell the maximum variation is ~0.02 Å, whilst the thermal contribution is ~0.18 Å. These values clearly indicate that for all of the alloys considered in this study the thermal component dominates the magnitude of PDF peak width. In addition, as the alloys are not at the same homologous temperature, an estimation of the static component made in this manner is likely to be an overestimate in the case of CrMnFeCoNi. However, it is possible to compare this value to one that might be expected from an average hard sphere structure using r_{av} with static displacements of $\delta r \times r_{av}$. Using this approach, the expected magnitude of the static displacement in CrMnFeCoNi would be ~0.025 Å, which is of a similar magnitude to that of the observed variation of the first PDF peak width, indicating that this alloy does not contain an anomalous level of static lattice displacement.

Using the same approach, it is possible to estimate the expected magnitude of the static displacement of a highly strained version of the lattice. At present, the magnitude of the static displacement that constitutes a highly strained lattice has not been quantitatively defined, which makes evaluation of the concept difficult. However, the δr parameter has been widely used to assess the stability of the solid solution phases in HEAs and a working limit of 0.066 (i.e. 6.6%) has been suggested, beyond which amorphisation would be expected [18]. It should be noted that the magnitude of this value is approximately the same as that derived from the Hume-Rothery rules for an equiatomic binary alloy with a 15% difference in atomic radii. For CrMnFeCoNi, a δr of 0.066 would lead to a static displacement of ~0.17 Å, which is far greater than that estimated from the experimental data and is on the order of the observed dynamic displacements. However, it is important to realise that this approach is very simplistic and does not take into account any factors apart from atomic radii. To address this, detailed calculations using first-principles approaches would be required to provide a more accurate assessment of the effect of static displacements on PDF peak widths.

Without being able to accurately separate the dynamic and static displacements it is impossible to determine the exact contribution of each component, but, clearly, neither can be ignored. The PDF peak widths of the HEA were generally the greatest within the alloys considered, which, in terms of a static displacement would suggest that the HEA lattice contains the most local strain. However, the widths of these PDF peaks were not disproportionately greater than those of Ni-33Cr or Ni-37.5Co-25Cr. In addition, the dynamic displacements due to thermal motion would be expected to be greatest in the HEA as it has the lowest melting temperature. Thus, the level of static displacements required to rationalise the observed peak widths would be lower. As a result, the current data indicated that whilst substitution of different elements into a pure metal leads to a local strain, there is no clear evidence that the level of strain is anomalously large for the equiatomic CrMnFeCoNi HEA. The comparable level of peak definition at high-r in all of the obtained PDFs further supports this assertion.

This conclusion is contrary to one of the four original core principles of HEAs and challenges the concept that the lattices of multiple principal element solid solutions are, by necessity, highly distorted. However, this result is perhaps unsurprising given the extremely small variations in atomic radii of the constituent elements. Further detailed measurements should be performed on alternative single phase alloys that contain elements with greater

variations in atomic radii. In addition, to enable a more rigorous analysis of local strain, a quantitative description of what constitutes a highly distorted lattice is required.

5. Conclusions

The level of local lattice strain in six single phase face-centered cubic materials, with varying compositional complexity, has been studied through neutron based total scattering measurements to assess the level of distortion present in the CrMnFeCoNi HEA.

Rietveld refinement of the Bragg data and reverse Monte-Carlo modelling of the total scattering data both indicated that, in the condition studied, all of the alloys were statistically random solid solutions. None of the Bragg data exhibited pronounced dampening, which would be expected for a highly distorted lattice, and the observed variations in the U_{iso} parameter could be rationalised simply in terms of homologous temperatures.

The PDFs obtained from the total scattering measurements were similar for all of the materials considered. The definition of the peaks in each PDF was maintained to high r values in all cases, suggesting that there were no significant deviations of the atoms from the space lattice sites in any of the alloys.

Detailed analysis of the PDF peak widths corresponding to the first six coordination shells was used to assess the extent of local lattice strain in the different materials. In general, the HEA was found to have the broadest peaks, which could suggest the highest level of local lattice strain within the materials studied. However, the peaks were not markedly broader than those of Ni-33Cr or Ni-37.5Co-25Cr, indicating that the level of strain was not disproportionately larger than those present in the other alloys. In addition, the width of a PDF peak is also dependent upon the magnitude of the thermal oscillations of the atoms within the lattice, which would be greater at higher homologous temperatures. Since the HEA has the lowest melting temperature of the materials considered, it would exhibit the greatest level of thermal broadening, which, consequently, would reduce the extent of local lattice strain required to rationalise a given PDF peak width. As such, the data presented here finds no clear evidence that the local lattice strain in the equiatomic CrMnFeCoNi HEA is anomalously large.

Acknowledgements

The authors would like to thank K. Christofidou, K. Roberts and S. Rhodes for their assistance, the Science and Technology Facilities Council for providing access to the Polaris instrument at ISIS (RB1520332) and the EPSRC/Rolls-Royce Strategic Partnership for funding (EP/M005607/1 and EP/H022309).

References

[1] J. Yeh, S. Chen, S. Lin, J. Gan, T. Chin, T. Shun, C. Tsau, S. Chang, Nanostructured high-entropy alloys with multiple principal elements: novel alloy design concepts and outcomes, Adv. Eng. Mater. 6 (2004) 299.
[2] J.W. Yeh, S.J. Lin, T.S. Chin, J.Y. Gan, S.K. Chen, Formation of simple crystal structures in Cu-Co-Ni-Cr-Al-Fe-Ti-V alloys with multiprincipal metallic elements, Metall. Mater. Trans. A 35 (2004) 2533.
[3] C. Tong, Y. Chen, S. Chen, J. Yeh, T. Shun, C. Tsau, S. Lin, S. Chang, Microstructure characterization of AlxCoCrCuFeNi high-entropy alloy system with multiprincipal elements, Metall. Mater. Trans. A 36A (2005) 881.
[4] C.-C. Tung, J.-W. Yeh, T.-T. Shun, S.-K. Chen, Y.-S. Huang, H.-C. Chen, On the elemental effect of AlCoCrCuFeNi high-entropy alloy system, Mater. Lett. 61 (2007) 1.
[5] B. Cantor, I.T.H. Chang, P. Knight, A.J.B. Vincent, Microstructural development in equiatomic multicomponent alloys, Mater. Sci. Eng. A 375–377 (2004) 213.
[6] N.G. Jones, A. Frezza, H.J. Stone, Phase equilibria of an Al0.5CrFeCoNiCu high entropy alloy, Mater. Sci. Eng. A 615 (2014) 214.
[7] F. Zhang, C. Zhang, S.L. Chen, J. Zhu, W.S. Cao, U.R. Kattner, An understanding of high entropy alloys from phase diagram calculations, Calphad 45 (2013) 1.
[8] E.J. Pickering, H.J. Stone, N.G. Jones, Fine-scale precipitation in the high-entropy alloy Al0.5CrFeCoNiCu, Mater. Sci. Eng. A 645 (2015) 65.
[9] X.D. Xu, P. Liu, S. Guo, A. Hirata, T. Fujita, T.G. Nieh, C.T. Liu, M.W. Chen, Nanoscale phase separation in a fcc-based CoCrCuFeNiAl0.5 high-entropy alloy, Acta Mater. 84 (2015) 145.
[10] J.-W. Yeh, Recent progress in high-entropy alloys, Ann. de chimie - Sci. des Materiaux 31 (2006) 633.
[11] J.W. Yeh, Physical metallurgy of high-entropy alloys, JOM 67 (2015) 2254.
[12] E.J. Pickering, N.G. Jones, High entropy alloys: a critical assessment of their founding principles and future prospects, Int. Mater. Rev. (2016, **61** (3), 183–202).
[13] F.J. Wang, Y. Zhang, G.L. Chen, Atomic packing efficiency and phase transition in a high entropy alloy, J. Alloys Compd. 478 (2009) 321.
[14] C.-W. Tsai, Y.-L. Chen, M.-H. Tsai, J.-W. Yeh, T.-T. Shun, S.-K. Chen, Deformation and annealing behaviors of high-entropy alloy Al0.5CoCrCuFeNi, J. Alloys Compd. 486 (2009) 427.
[15] J.-W. Yeh, S.-Y. Chang, Y.-D. Hong, S.-K. Chen, S.-J. Lin, Anomalous decrease in X-ray diffraction intensities of Cu–Ni–Al–Co–Cr–Fe–Si alloy systems with multi-principal elements, Mater. Chem. Phys. 103 (2007) 41.
[16] O.N. Senkov, D.B. Miracle, Effect of the atomic size distribution on glass forming ability of amorphous metallic alloys, Mater. Res. Bull. 36 (2001) 2183.
[17] A. Inoue, Stabilization of metallic supercooled liquid and bulk amorphous alloys, Acta Mater. 48 (2000) 279.
[18] X. Yang, Y. Zhang, Prediction of high-entropy stabilized solid-solution in multi-component alloys, Mater. Chem. Phys. 132 (2012) 233.
[19] Y. Zou, S. Maiti, W. Steurer, R. Spolenak, Size-dependent plasticity in an Nb25Mo25Ta25W25 refractory high-entropy alloy, Acta Mater. 65 (2014) 85.
[20] K. Huang, X-ray reflexions from dilute solid solutions, Proc. R. Soc. A Math. Phys. Eng. Sci. 190 (1947) 102.
[21] B.E. Warren, B.L. Averbach, B.W. Roberts, Atomic size effect in the X-ray scattering by alloys, J. Appl. Phys. 22 (1951) 1493.
[22] M.-H. Tsai, J.-W. Yeh, High-entropy alloys: a critical review, Mater. Res. Lett. 2 (2014) 107.
[23] W.-R. Wang, W.-L. Wang, S.-C. Wang, Y.-C. Tsai, C.-H. Lai, J.-W. Yeh, Effects of Al addition on the microstructure and mechanical property of AlxCoCrFeNi high-entropy alloys, Intermetallics 26 (2012) 44.
[24] W. Guo, W. Dmowski, J.-Y. Noh, P. Rack, P.K. Liaw, T. Egami, Local atomic structure of a high-entropy alloy: an X-ray and neutron scattering study, Metall. Mater. Trans. A 44 (2012) 1994.
[25] Santodonato LJ, Zhang Y, Feygenson M, Parish CM, Gao MC, Weber RJK, Neuefeind JC, Tang Z, Liaw PK. Deviation from high-entropy configurations in the atomic distributions of a multi-principal-element alloy. Nat. Commun. 1;6:1.
[26] H. Diao, L.J. Santodonato, Z. Tang, T. Egami, P.K. Liaw, Local structures of high-entropy alloys (HEAs) on atomic scales: an overview, Jom (2015, **67** (10), 2321–2325).
[27] L.R. Owen, H.Y. Playford, H.J. Stone, M.G. Tucker, A new approach to the analysis of short-range order in alloys using pair distribution functions, Acta Mater. (2016). **115**, 155–166.
[28] O. Arnold, J.C. Bilheux, J.M. Borreguero, A. Buts, S.I. Campbell, L. Chapon, M. Doucet, N. Draper, R.F. Leal, M.A. Gigg, V.E. Lynch, A. Markvardsen, D.J. Mikkelson, R.L. Mikkelson, R. Miller, K. Palmen, P. Parker, G. Passos, T.G. Perring, P.F. Peterson, S. Ren, M.A. Reuter, A.T. Savici, J.W. Taylor, R.J. Taylor, R. Tolchenov, W. Zhou, J. Zikovsky, Mantid—Data analysis and visualization package for neutron scattering and μ SR experiments, Nucl. Inst. Methods Phys. Res. A 764 (2014) 156.
[29] A.C. Larson, R.B. Von Dreele, General structural analysis system (GSAS), LAUR 86–748, 1994.
[30] A.K. Soper, GudrunN and GudrunX : Programs for Correcting Raw Neutron and X-ray Diffraction Data to Differential Scattering Cross Section, Rutherford Appleton Laboratory Technical Report, RAL-TR-2011-013, 2011.
[31] M.G. Tucker, D.A. Keen, M.T. Dove, A.L. Goodwin, Q. Hui, RMCProfile: reverse Monte Carlo for polycrystalline materials, J. Phys. Condens. Matter 19 (2007) 335218.
[32] B. Borie, X-ray diffraction effects of atomic size in alloys, Acta Crystallogr. 10 (1957) 89.
[33] B.D. Cullity, Elements of X-ray Diffraction, Addison-Wesley Publishing Company, 1956.
[34] I.K. Jeong, R.H. Heffner, M.J. Graf, S.J.L. Billinge, Lattice dynamics and correlated atomic motion from the atomic pair distribution function, Phys. Rev. B 67 (2003) 104301.
[35] E.J. Pickering, R. Muñoz-Moreno, H.J. Stone, N.G. Jones, Precipitation in the equiatomic high-entropy alloy CrMnFeCoNi, Scr. Mater. 113 (2016) 106.